Effect of electrode resistance on dielectric and transport properties of multiferroic superlattice: A Impedance spectroscopy study

Sandra Dussan, Ashok Kumar, J. F. Scott, and Ram S. Katiyar

Citation: AIP Advances **2**, 032136 (2012); doi: 10.1063/1.4746026
View online: http://dx.doi.org/10.1063/1.4746026
View Table of Contents: http://aipadvances.aip.org/resource/1/AAIDBI/v2/i3
Published by the American Institute of Physics.

Effect of electrode resistance on dielectric and transport properties of multiferroic superlattice: A Impedance spectroscopy study

Sandra Dussan,[1] Ashok Kumar,[1,2,a] J. F. Scott,[1,3] and Ram S. Katiyar[1,a]
[1]*Department of Physics and Institute for Functional Nanomaterials, University of Puerto Rico, San Juan, Puerto Rico 00931-3343, USA*
[2]*National Physical Laboratory, Council of Scientific and Industrial Research (CSIR), New Delhi 110 012, India*
[3]*Cavendish Laboratory, Dept. Physics, Cambridge University, Cambridge CB3 0HE, U.K.*

(Received 28 May 2012; accepted 30 July 2012; published online 9 August 2012)

Fundamental microscopic processes that take place throughout of ferroelectric $PbZr_{1-x}Ti_xO_3$ (x = 0.48) (PZT) and ferromagnetic $La_{1-x}Sr_xMnO_3$ (x = 0.33) (LSMO) superlattices (SLs) architecture including the influences of electrode on functional properties are analyzed using impedance spectroscopy technique (IS). Temperature and frequency dependence impedance and ac conductivity are investigated in the ranges of 100–600 K and 10^2–10^6 Hz suggesting a strong dependence between temperature and electrode contribution in the electrical properties. The results are interpreted using the alternative Z′ as a function of Z″/F representation, more commonly this representation applied in the cases when the complex impedance curves show overlapped arcs due to the relative small differences in relaxations frequencies. Activation energy is obtained from the Arrhenius plot of relaxation time and ac conductivity in order to identify the conduction mechanism present in the superlattices. [http://dx.doi.org/10.1063/1.4746026]

I. INTRODUCTION

In the last years, there has been growing scientific interest in tailoring materials for the coexistence of two or more ferroic properties (multiferroics),[1,2] and the associated coupling between them allowing additional degree of freedom based on magnetic control of ferroelectric polarization as well as electrically tuned magnetization with practical applications in the designing of devices, such as transducers, actuators, magnetic field sensors and memory storage elements.[3–5] The development in growth technique of thin film offers a versatile approach to fabricate superlattice heterostructure that allow combining different ferroic phases in the same superlattice cells.[6] The oxide perovskite family is a promising candidate materials to construct multiferroic supertlattices (MSLs) whose structure consist of alternating ferroelectric (FE) and ferromagnetic (FM) layers. In this context, there is a general interest in $PbZr_xTi_{1-x}O_3$, since it has excellent FE and piezoelectric properties, with high Curie temperature (T_C), additionally their degree of versatility that lies in the tunability of the lattice parameter and physical properties due to the Zr/Ti composition ratio, make this material a potential candidate to use in non-volatile random access memories.[7,8] On the other hand, maganites such as $La_xSr_{1-x}MnO_3$ is a good candidate as ferromagnetic layer and as the conducting bottom electrode for its colossal magnetoresistance properties, half-metallic behavior and high Curie temperature of about 370 K.[9,10] Several of these systems have been reported in literature, such as $La_{0.6}Sr_{0.4}MnO_3$/0.7$Pb(Mg_{1/3}Nb_{2/3})O_3$–0.3$(PbTiO_3)$,[11]

[a]Author to whom correspondence should be addressed: Ashok Kumar; Electronic mail: (ashok553@gmail.com); R S Katiyar; Electronic mail: (rkatiyar@uprrp.edu).

TABLE I. Relations between the four basic complex functions. Where $j = \sqrt{-1}$, ω is the angular frequency ($\omega = 2\pi f$), $C_0 = \varepsilon_0 A/d$ is the vacuum capacitance with ε_0 the permittivity of the free space (8.854×10^{-12} F/m), d and A, are the thickness and area of electrode deposited on the sample, respectively.

	Z*	Y*	M*	Є*
$Z^* = Z' - jZ''$	Z*	$(Y^*)^{-1}$	$(j\omega C_0)^{-1} M^*$	$(j\omega C_0)^{-1} (Є^*)^{-1}$
$Y^* = Y' + jY''$	$(Z^*)^{-1}$	Y*	$j\omega C_0 (M^*)^{-1}$	$j\omega C_0 Є^*$
$M^* = Y' + jY''$	$j\omega C_0 Z^*$	$j\omega C_0 (Y^*)^{-1}$	M*	$(Є^*)^{-1}$
$Є^* = Є' - j Є''$	$(j\omega C_0)^{-1}(Z^*)^{-1}$	$(j\omega C_0)^{-1} Y^*$	$(M^*)^{-1}$	Є*

$La_{0.7}Sr_{0.3}MnO_3/PbZr_xTi_{1-x}O_3$,[12] $Pb(Zr_{0.2}Ti_{0.8})O_3/La_{1-x}Sr_xMnO_3$,[13] and our previous report on PZT/LSMO bilayer and superlattices (SLs) thin films.[14,15]

There are many factors which influence the (SLs) properties, such as nature of the constituent materials, their thickness, surface morphology, lattice mismatch, interface structure between the sublayers, and the substrate. In most cases relies of the role that play the interfaces and electrodes and how they influence its behavior. At the interface, physical properties, crystallographic, mechanical, compositional, and, particularly, electrical response, change precipitously and heterogeneous charge distributions (polarizations) reduce the overall electrical conductivity of a system. The impedance spectroscopy (IS),[16] is a powerful experimental method to separate and study the electrical process in a system, which occurring between electro-active regions and their interfaces when it is applying an ac signal as an input perturbation. The output response allows distinguishing between intrinsic (bulk or grain) and extrinsic contributions (grain boundary, surface layer, and electrode). The ac impedance method allows a complete interpretation of the frequency dependent electrical properties. The data can be analyzed in terms of four possible complex formalisms, the impedance Z*, admittance Y*, electric modulus M*, and relative permittivity Є*, which are related as to one another according the Table I.

In the impedance spectroscopy technique, a sinusoidal signal of low amplitude is applied across a sample and the impedance (Z*) and phase shift (θ) are measured directly at the output. The display of impedance data in the complex plane appears in the form of a succession of semicircles attributed to relaxation phenomena with enough different time constants to allow the separation of each contribution: (i) high frequency region is due to grains; (ii) intermediate frequency due to the grain-boundary and (iii) low frequency region due to material-electrode interface. This technique has been applied to analyze the electrical-microstructure relationship of several multiferroics composites.[17–20]

We report the use the IS technique to gain an understanding of the physical phenomena occurring in the (PZT) and (LSMO) SLs system, by using an appropriate equivalent circuit as a framework.

II. EXPERIMENTAL DETAILS

Superlattices (SLs) of PZT and $La_{0.67}Sr_{0.33}MnO_3$ with a periodicity of 5nm/1 nm were fabricated onto $LaAlO_3$ substrates by pulsed laser deposition technique from individual stoichiometric ceramic targets of PZT and LSMO, synthesized by a conventional solid-state reaction route. A KrF excimer laser (240 nm) with a laser energy density of 1.8 J/cm^2 and repetition rate of 10 Hz was used to deposit the SLs thin films. The temperature of deposition was kept at 600°C under an oxygen pressure of 80 mTorr, followed by annealing at 700°C for 30 min in oxygen atmosphere. Finally, the films were cooled down to room temperature at a slow rate. An in-situ reflection high energy electron diffraction (RHEED) system was employed to monitor the growth of SLs at 24 keV beam energy, 1.4 A filament current and with azimuthal angle less than 5°. The total thickness of 360 ± 10 nm was measured using an ambios xp-200 profilometer. The crystallographic structural analysis was done with a Bruker D8 discover x-ray diffractometer system using a characteristic X-ray of Cu-Kα. In order to examine the topography and surface roughness a scanning probe microscopy Veeco-AFM contact mode was used. For the electrical measurements top electrodes were deposited by a shadow mask in dc-sputtering with an area of 1×10^{-4} cm^2. The complex impedance measurements were

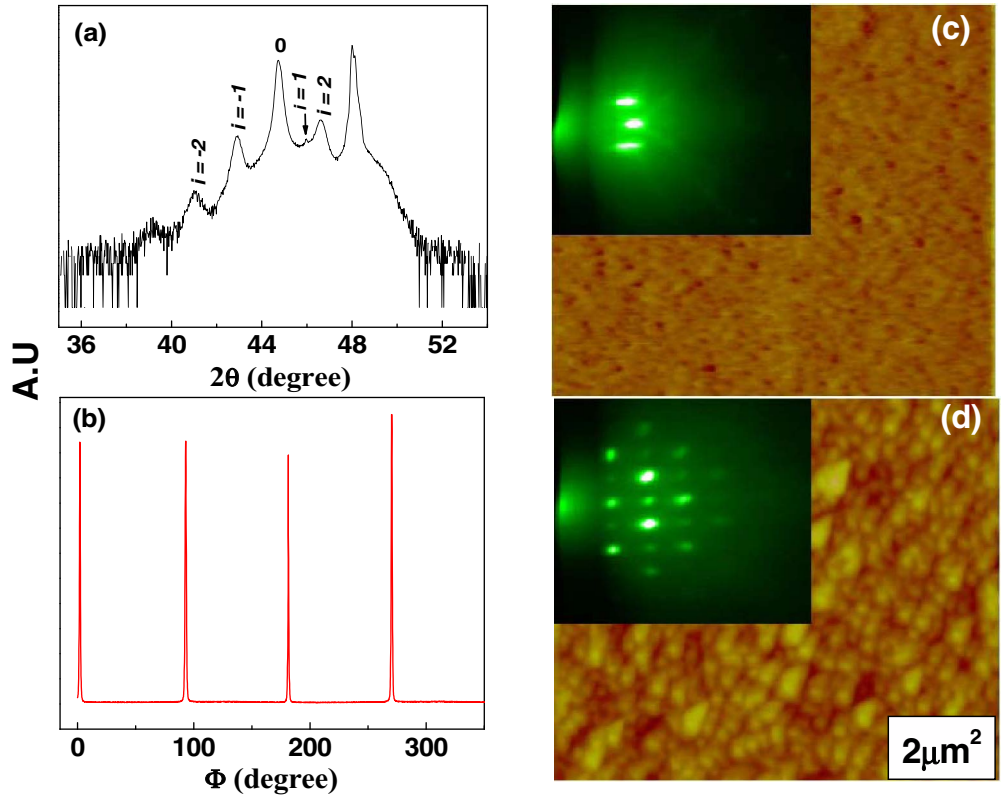

FIG. 1. Room temperature (a) θ-2θ x-ray diffraction (XRD) pattern, (b) Φ-scan around (202) and (220) reflections of $PbZr_{0.52}Ti_{0.48}O_3$ (PZT)/$La_{0.67}Sr_{0.33}MnO_3$ (LSMO) superlattices (SLs) on LAO substrate. $2\,\mu m \times 2\,\mu m$ AFM topography images and RHEED pattern (inset the left upper corner) of (c) LSMO (bottom) and (d) SLs system on LAO substrates respectively.

carried out between 100 Hz an 1 MHz varying the temperature from 100 K to 600 K were carry out using an HP4294 impedance analyzer and a temperature controller (K-20 MMR technologies, Inc.)

III. RESULTS AND DISCUSSION

A. Structure

The θ-2θ x-ray scan around (200) fundamental peak (35°–55° in 2θ) shows the presence of higher order satellite peaks denoted by *i* that corresponds to *i-th* satellite peak, clearly indicates that the superlattice architecture with a periodic modulation (Λ) of the constituent was achieved (see Fig. 1(a)). The calculated modulation period of 6 nm was done from the following Bragg relation:

$$\Lambda = \frac{\lambda}{2(\sin\theta_{i+1} - \sin\theta_i)} \tag{1}$$

Where λ is the x-ray Cu-k_α wavelength (1.54 Å), θ_{i+1}, and θ_i are the angular position of two adjacent SLs satellite peaks. One may note that 360 nm thick superlattice structures with 6 nm periodicity (5 nm/1 nm) should display ideally the XRD patterns with 60 superperiod. Unfortunately we have not observed all the superperiods due to very high intensity (counts/second) of the substrate and the experimental limitation of the θ-2θ scan powder diffraction x-ray equipment. To study in-plane crystallographic alignment of the SLs on LAO (100), a Φ scan (Fig. 1(b)) was realized around (202) plane with the axis normal to the plane of the substrate. Four peaks at the interval of 90° spacing from each other are clearly observed, indicating the fourfold symmetry. The scan shows, with the same rotation angles as those of the LAO (220) which confirms that the SLs grown cubic-on cubic epitaxy.

The surface morphology of bottom electrode (LSMO onto 100-LAO) and SLs were investigated by AFM images, as shown in Figs. 1(c) and 1(d) respectively. It can be seen that the surface of bottom LSMO film is very smooth and uniform, with average roughness of 0.39nm, while the SLs surface exhibit an increase of the grain size and average roughness (1.34 nm) compare with the bottom film. The RHEED pattern of the LSMO and SLs thin films are shown inset Figures 1(c) and 1(d) on the top left. The incident electron beam was along LAO (100). A series of clear bright diffraction spots lying on a Laue arc, corresponding to the intersection of the Laue sphere with the two-dimensional reciprocal rod lattice and the Kikuchi lines[21] were observed (inset Fig. 1(c)), revealing smoothness, well-ordered and atomically flat surface of LSMO (bottom) film. In the case of SLs films, as shown inset Fig. 1(d), around instead of streak-like diffraction spots indicate that the surface become rather rougher as compared with very smooth surface of the bottom LSMO layer, these results are in agreement with those obtained from AFM images. The results strongly confirm the perfect growth in-plane epitaxial of the samples onto (100)-LAO substrates. The various factors which influence the SLs structures and their functional properties are well explained by the P. Murugavel *et al.*.[22] The lattice mismatch (ε) between the substrate and the SLs film is the most significant source of the strain in the system which can be calculated from the relation:

$$\varepsilon = \left[\frac{a_{sub} - a_{film}}{a_{sub}}\right] \times 100\% \tag{2}$$

With a_{sub} and a_{film} as the lattice constant of the substrate and the SLs thin film respectively. We observed a compressive in-plane strain of ~ -4.93 % between bottom electrode and SLs. The bottom also experiences a compressive strain of $\sim -1.58\%$ with the LAO substrate. In fact the entire set of the SLs revealed an in-plane compressive stress, which is higher when increasing the periodicity of the SLs, this observed strain values indicate a higher degree of electrostriction across the interfaces which could generate strain mediated magneto-electric (ME) coupling.

B. Impedance Analysis

An appropriate choice of an equivalent circuit is important to interpret the experimental data that provides a realistic representation of the electrical properties of the material. In practice, it is very common to get more than one circuit that fitting good with the obtain data, but only one of these fits represent the real electrical and microstructure relationship. The most common ideal equivalent circuit consisting of two or three parallel resistor-capacitor (RC) elements connected in series, one represent the grain effects, the other represents the grain boundary and in some cases the presence of additional electroactive regions such as sample-electrode contribution. It is also common to use constant phase element (CPE) in the equivalent circuit which represent hybrid state of the circuit elements, as we know, in the real world not a single matter can exist in pure or ideal resistor, capacitor or inductor form.[16] For the data analysis the real Z' and the imaginary Z'' parts of the complex impedance Z* were obtained using the relations:

$$Z' = Z\cos\theta, \tag{3}$$

$$Z'' = Z\sin\theta. \tag{4}$$

The Figure 2(a) and 2(b) show the variations of Z' and Z'' as a function of the frequency at different temperatures (Inset low temperatures). The curves in the high frequency region appeared to merge with another, indicating the disappearance of space-charge polarization. Below 300 K, the peak moves out of our experiment frequency window, but around 500 K the peak occur and shifts to higher frequencies on increasing the temperature. According to the analysis of impedance spectra via the equivalent circuit, we fitted Z'' and Z' Vs. log f, using a circuit of a series array of two (low temperature) and three (high temperature) subcircuits, each of which consist of a resistor (R) and capacitor (C) join in parallel, then the equation for the impedance Z* for this circuit is given by:[23,24]

$$Z^* = \frac{1}{R_g^{-1} + i\omega C_g} + \frac{1}{R_{gb}^{-1} + i\omega C_{gb}} + \frac{1}{R_{ele}^{-1} + i\omega C_{ele}} = Z' + iZ'' \tag{5}$$

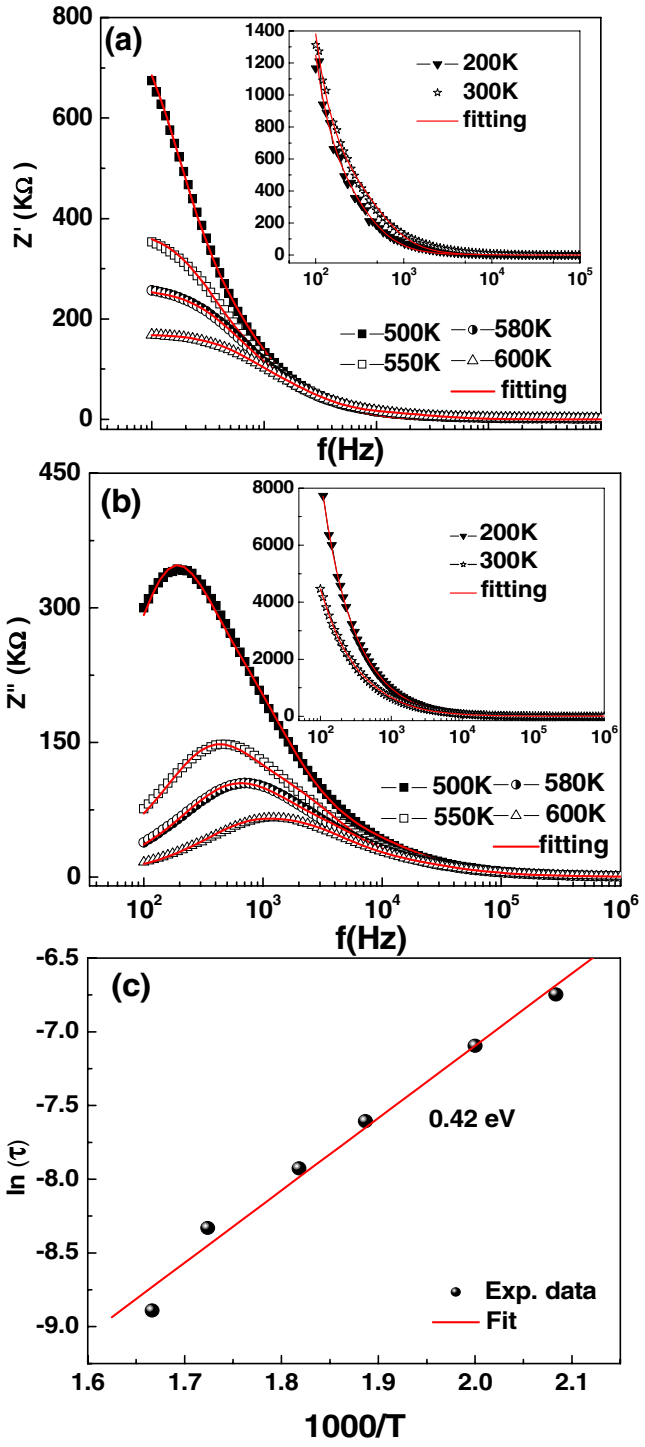

FIG. 2. Frequency dependent of, (a) Real Z′ and (b) Imaginary Z″ impedance for PZT/LSMO SLs system from 100 Hz to 10^6 Hz at high and low (inset) temperatures. (c) Variation of dielectric relaxation time τ with the temperature, the continuous line is the equivalent circuit fit and linear fit respectively.

Where

$$Z' = \frac{R_g}{1+(\omega R_g C_g)^2} + \frac{R_{gb}}{1+(\omega R_{gb} C_{gb})^2} \tag{6}$$

$$Z' = \frac{R_g}{1+(\omega R_g C_g)^2} + \frac{R_{gb}}{1+(\omega R_{gb} C_{gb})^2} + \frac{R_{ele}}{1+(\omega R_{ele} C_{ele})^2} \tag{7}$$

$$Z'' = R_g \left[\frac{\omega R_g C_g}{1+(\omega R_g C_g)^2}\right] + R_{gb}\left[\frac{\omega R_{gb} C_{gb}}{1+(\omega R_{gb} C_{gb})^2}\right] \tag{8}$$

$$Z'' = R_g \left[\frac{\omega R_g C_g}{1+(\omega R_g C_g)^2}\right] + R_{gb}\left[\frac{\omega R_{gb} C_{gb}}{1+(\omega R_{gb} C_{gb})^2}\right] + R_{ele}\left[\frac{\omega R_{ele} C_{ele}}{1+(\omega R_{ele} C_{ele})^2}\right] \tag{9}$$

The corresponding (*g, gb, ele.*) subscripts refers at the grain or bulk, grain boundary and electrode-sample interface elements respectively. At low temperature (100 K ≤ 400 K) the impedance we can fit with the equation (6) and (8) attributed to the grain and grain boundary, although the peaks of both elements already moved out of our experimental frequency windows. When the temperature is increased (400 K ≤ 600 K) we have to fit added another circuit element corresponding at the electrode-sample inter-phase contribution; in this case we use the equations (7) and (9) for Z′ and Z″ respectively. The magnitude in both profiles is seen to decrease with rise the temperature exhibiting a peak broadened, indicating Arrhenius type temperature dependence in the SLs system. The activation energy associated with the relaxation process is determined by fitting the Arrhenius plot (see Fig. 2(c)) in the temperature range (480 K ≤ T ≤ 600 K) using the relation:

$$\tau = \tau_o \, exp\left[\frac{-E_a}{k_B T}\right] \tag{10}$$

Where τ_o is the prefactor, E_a is the activation energy for relaxation process and k_B is the Boltzmann constant and T is the absolute temperature. It is observed that the relaxation time decreases when increase in temperature, indicating that the relaxation phenomenon is thermally activated. The obtained E_a value of 0.42 eV is in the range corresponding to the activation energy of electronic contribution calculated for multiferroic thin films.[25] The response of these circuits in the two complex plots in the form of the Cole-Cole (or Nyquist) representation at different temperatures is shown in Figure 3(a). At low temperature (Inset Figure 3(a).) the plot Z″ vs. Z′ linearly line up towards Z″ axis with large slope indicating high resistivity of the sample; as the temperature increases the curves become in semicircular arcs with a decreasing in the radii curvature exhibiting a reduction in the total resistance. From such plot it is feasible to extract the overall resistance R_T which is 354, 259 and 168 KΩ for 500, 550 and 600 K respectively. In order to confirm that the effectively the curves contained two or more overlapped arc as a consequence of more than one contribution in the electrical behavior which was shown with the fit done with the equivalent circuit using the equations (6)–(9), we use an alternative approach of the impedance spectra proposed by Abrantes *et al.*[26] This work uses representations of Z′ as a function of Z″/f plot; transforming the usual semicircles of the Nyquist plots into linear segments, where the slope is related to the relaxation frequency of each specific contribution (grain, grain boundary or electrode process) and the interception is related with the respective resistance. Figure 3(b) shows the corresponding Z′ vs. Z″/*f* plot obtained at 600 K with the respective relaxation frequency of 1.42 KHz, 717 Hz and 430 Hz for grain, grain boundary and electrode respectively. The interceptions obtained by extrapolation of each branch are to close with the resistance values predicted by the fitting with the impedance electrical equations (6)–(9), which are listed in the Table II. The resistance values for the electrode-inter-phase process increase when increase the temperatures, while than in the other two process grain and grain boundary, the values of the resistance tends to decrease with the temperature. Considering that for electrical measurement of our samples, these can be treated as serial nanocapacitors.[15] The obtained results indicate that the dielectric properties of the SLs become perturbed by the metallic- semi-metallic transition of the LSMO. Because when heated, these doped manganese compound (LSMO) show a large decrease

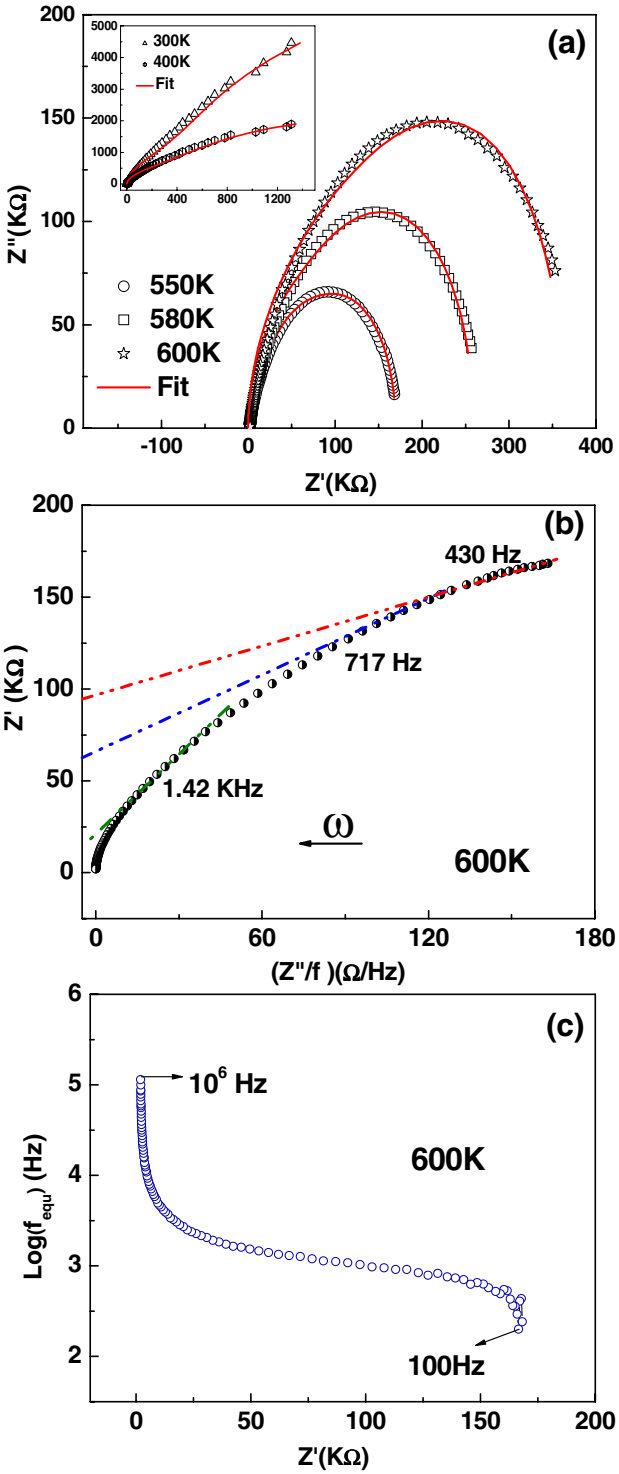

FIG. 3. (a) Complex impedance plane plots at high temperature regime (inset low temperature) and its corresponding (b) Z' vs. Z''/f and (c) Log f_{equ} vs. Z' representations, where $f_{equ} = dZ'/d\,(Z''/f)$.

TABLE II. Resistance values of grain (R_g), grain boundary (R_{gb}) and electrode-interface (R_{ele}) contribution of Impedance spectra for SLs determined by fitting data and by the intercept of each branch in Z'' vs. f and Z' vs. Z''/f plots respectively.

	R_g (KΩ)		R_{gb} (KΩ)		R_{elec} (KΩ)	
Temperature (K)	FIT	Extrapolation	FIT	Extrapolation	FIT	Extrapolation
550	94.86	94.61	205.19	205.39	63.63	62.50
580	49.76	49.76	135.19	133.26	74.12	74.11
600	12.65	13.00	65.31	65.90	90.44	82.52

in conductivity associated with a ferromagnetic to paramagnetic phase transition.[27] According them the plot of equivalent frequency f_{equ} vs. Z' Figure 3(c), where $f_{equ} = dZ'/d\,(Z''/f)$ shows a decay in the low frequency range that indicates the onset of electrode contribution. The sudden jump in the high frequency range corresponds to the transition from grain boundary to bulk (grain) contribution.

C. Ac conductivity study

The ac conductivity σ_{ac} was calculated from dielectric data using the empirical relation:

$$\sigma_{ac} = \omega \varepsilon_r \varepsilon_0 \tan\delta \tag{11}$$

Where, ε_r, tan δ, ε_0 and ω are the dielectric permittivity, the dissipation factor, permeability of the free space and the angular frequency respectively. The ac conductivity (σ_{ac}) of the SL film has been measured as a function of frequency at different temperatures and is shown in Figure 4(a). From the plot, we observed the following characteristics in the dynamic conductivity: (i) at sufficient low frequencies and low temperatures, the ac conductivity was almost frequency independent, which are representative of dc leakage current throughout the sample; (ii) frequency dependent plateau in the mid and high frequencies regions are exhibited; (iii) dispersion and merging trend of the ac conductivity curves at all frequencies spectrum, with the increase the temperature; (iv) In the high frequency regime ($>10^4$ Hz) at high temperatures (>400 K) a shoulder is observed; (v) there is an overall increase in the conductivity with the measuring frequency and temperature, that is more obvious below 400 K. In order to analyze the frequency dependence of conductivity, a conventional formalist used for that, is based on the power law proposed by Jonscher[28,29]

$$\sigma(\omega) = \sigma_0 + A\omega^s \tag{12}$$

Where σ (ω) is the total electrical conductivity, σ_0 is frequency-independent conductivity (which is related to dc conductivity), A is the temperature dependent pre-exponential factor and s is frequency exponent ($0 < s < 1$). In the present study we observed that the results do not follow the simple power relation given by (12). It is clear from inset Fig. 4(a) that, after the dc plateau (region I) two different kinds of relaxations are encountered: at low and intermediate frequency dispersion (region II) associated with the electrode and grain boundary effects, and the region III at high frequency one, with grain contribution, which are agree with the results obtained from the impedance analysis. According with the above mentioned, current data have been studied using the jump relaxation model (JRM),[30] this model is based in following idea: after a hop of a central ion from a initially relaxed local configuration this ion is no longer in equilibrium with its surroundings; in order to stabilize the new position of the ion, the others ions its environment have to move. On the other hand, the ion can also jump back (unsuccessful hop) in order to (partially) relax the configuration after the jump. The conductivity in the low frequency region is associated with successful hop, which is attributed to the long-range translational motion of ions, and therefore contributing to dc conductivity. As the frequency increases (>10 KHz) the unsuccessful hops increases, since two different kinds of relaxation process take place, such as; the correlated ion position related to forward backward forward, i.e., unsuccessful hopping and the localized orientation hopping (once jumped ions become relaxed and stay in the new site), i,e., a successful hop. As the ratio of successful to unsuccessful hopping increases, results in more dispersive conductivity at higher frequencies. Applying the JRM to the frequency responds of the conductivity data for SLs system, it was possible

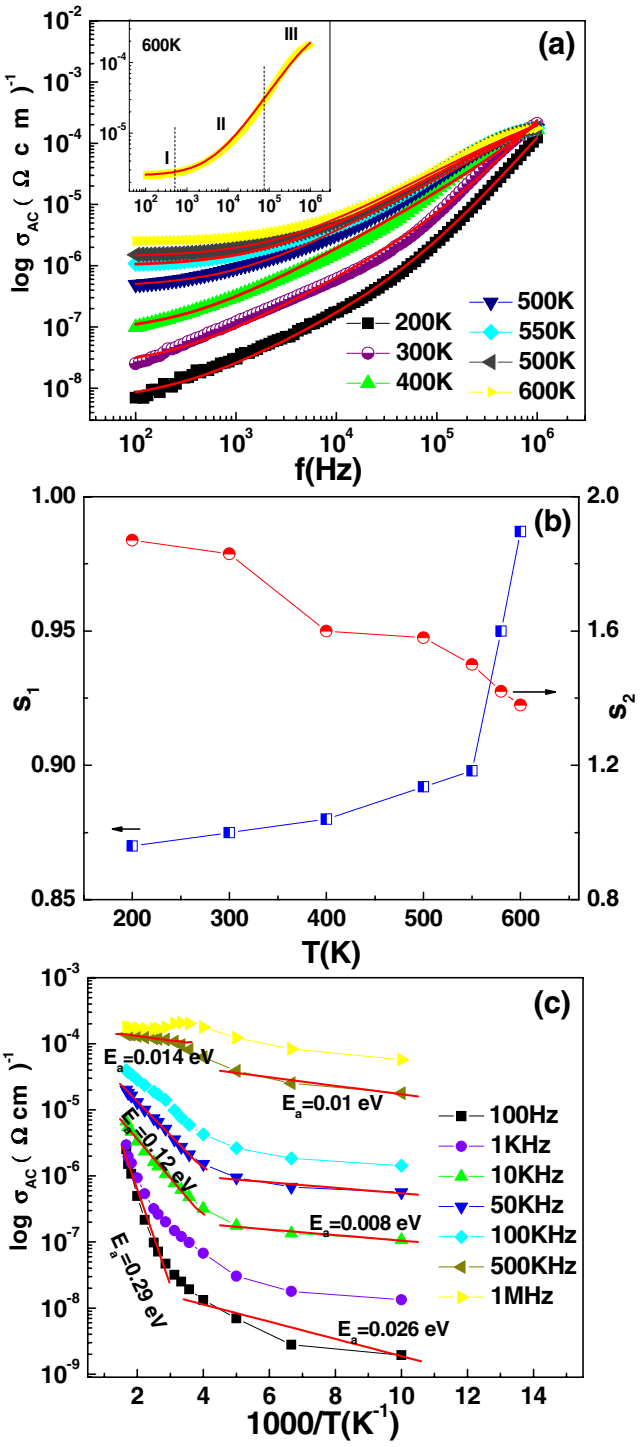

FIG. 4. (a) Frequency dependent of ac conductivity and its continuous fitting curves using double power law (inset illustration of different frequencies regimes at 600 K). (b) Double power temperatures parameters (s_1,s_2) obtained from the fitting curve and (c) Arrhenius plots as a function of the temperature, indicating two regions with different activation energies.

fitted to a double power law;[30,31]

$$\sigma(\omega) = \sigma_0 + A_1\omega^{s_1} + A_2\omega^{s_2} \quad (13)$$

To describe the different contribution from the fitted data (Fig. 4(a), solid lines) according with the relation (13); the first term σ_0 correspond to dc conductivity, which translational hopping gives the long-range electrical transport in the long-time limit, (i.e., as the frequency approaches zero). The second term $A_1\omega^{s_1}$ is assigned to the middle region (II) in which the exponent $0 < s_1 < 1$ characterizes the low frequency regime corresponding to short rang translational hopping motion. The third term $A_2\omega^{s_2}$ corresponds at higher frequency region (III) for which the exponent $1 < s_2 < 2$ indicates the localized or reorientation hopping motion. The s_1 and s_2 values obtained from the fitting data are shown in Fig. 4(b) as a function of the temperature; these values varied between 0.87–0.926 and 1.43–187 respectively. The s_1 exhibit a continuous increase with the temperature whereas s_2 decrease in the measured temperature. Furthermore both of them show an abrupt increase and decrease respectively in the high temperature range ($T > 500$ K), which correspond to onset of the crossover from the grain boundaries contribution to electrode contribution well supported by impedance analysis. Since, early reports[30–32] predict the dependence of s with the frequency and temperature, where an increase of the exponent values with increasing temperature is ascribed to the small polaronic hopping, while the large polaronic hopping causes decrease in exponent values. From the trend of the exponents behavior with the temperature of SLs sample, we have obtained the value of s_1 less that 1 increasing in measured temperature, it can indicates that the conduction in region II attributed to the short translational hopping is assisted by small polaronic mechanism. On the other hand, in the case of s_2 the values fluctuate between 1and 2 and decreases with reach the temperature, in this case the conduction in region III ascribed to the localized orientation hopping, is assisted by large polaron mechanism. The thermal activation of the charge species contributing to ac conductivity is further explorer using the Arrhenius law, the corresponding Arrhenius equation is read as;

$$\sigma_{ac} = \sigma' \exp\left[\frac{-E_a}{KT}\right] \quad (14)$$

Where σ' is the pre-exponential factor of conductivity, E_a is the activation energy, K is the Boltzmann constant and T is absolute temperature. The activation energy E_a associated with the conduction mechanism in the analyzed temperature region at different frequencies calculated from the slope of the Log σ vs. 1/T curves is shown in Fig. 4(c). It is observed from the plot that there are divided into two different regions of activation energy. The values were found to vary between 0.29–0.014 and 0.026–0.08 eV for high and low temperature regions respectively. These E_a values increase with increase in temperature at a constant frequency; this can be attributed to more energy required to overcome the thermal fluctuation by the charge carriers at high temperature region. It also observed that the activation energy decrease on increasing frequency, this may be due to the fact that at low frequency regime the overall conductivity is due to the hopping–mobility-transportation of charge carriers over a large distance, while at high frequency regime hopping-transportation is restricted to only nearest neighboring defects sites, due smaller respond time available to respond to external field. On the other hand, it is of particular interest to mention that the temperature dependent dielectric curve exhibit an anomaly at higher frequency above the ferromagnetic to paramagnetic phase transition of the LSMO, that is closely related with some electrode-sample interface resistance and also the electrode resistance of nanocapacitors formed in the artificial superlattices.[15]

IV. CONCLUSIONS

We have successfully grown the high quality epitaxial PZT/LSMO thin films probed by Φ-scan, RHEED patterns and AFM topography. Frequency and temperature dependent impedance and conductivity spectra of multiferroic superlattices indicate the significant effect of electrode resistance on the electrical and functional properties. Equivalent circuit utilized to investigate the real and imaginary impedance data indicates two and three (grain, grain boundary and electrode-inter-phase) process contributions depending upon the temperature. These results are in agreement

with the contributions obtained from the alternative Z′ vs. Z″/f representations. The ac conductivity was found to obey well the double power law, exponent values ($s_1 < 1$ and $s_2 < 2$) indicating the different mobile charge species contribution to the conductivity. Temperature dependent ac conductivity follows the Arrhenius law and it has two different values of activation energy for different temperature due to different conduction mechanism.

ACKNOWLEDGMENTS

This work was partially supported by DoE FG 02-08ER46526 and DoD W911MF-11-1- 0204 grants to UPR. One of the authors S.D. acknowledges an IFN fellowship.

[1] H. Schmid, Ferroelectrics **162**, 317 (1994).
[2] N. A. Spaldin, S.-W. Cheong, and R. Ramesh, Phys. Today **63**(10), 38 (2010).
[3] W. Eerenstein, N. D. Mathur, and J. F. Scott, Nature (London) **442**, 759 (2006).
[4] J. F. Scott, Nature Mater. **6**, 256 (2007).
[5] N. Mathur, Nature **454**, 591 (2008).
[6] R. Ramesh and N. A Spaldin, Nature Mater. **6**, 21 (2007).
[7] J. F. Scott and C. A. P. D. Araujo, Science **246**, 1400 (1989).
[8] O. Auciello, J. F. Scott, and R. Ramesh, Phys. Today **51**(7), 22 (1998).
[9] A. Urushibara, Y. Moritomo, T. Arima, A. Asamitsu, G. Kido, and Y. Tokura, Phys. Rev. B **51**, 14103 (1995).
[10] J. H. Park, E. Vescoso, H. J. Kim, C. Kwon, R. Ramesh, and T. Venkatesan, Nature (London) **392**, 794 (1998).
[11] A. R. Chaudhuri, R. Ranjith, S. B. Krupanidhi, R. V. K. Mangalam, A. Sundaresan, S. Majumdar, and S. K. Ray, Journal of Applied Physics **101**, 114104 (2007).
[12] M. Ziese, A. Setzer, I. Vrejoiu, B. I. Birajdar, B. J. Rodriguez, and D. Hesse, J. Appl. Phys. **104**, 063908 (2008).
[13] C. A. F. Vaz, Y. Segal, J. Hoffman, F. J. Walker, and C. H. Ahn, J. Vac. Sci. Technol. B **28**(4), C5A6 (2010).
[14] S. Dussan, A. Kumar, J. F. Scott, and R. S. Katiyar, Appl. Phys. Lett. **96**, 072904 (2010).
[15] S. Dussan, A. Kumar, J. F. Scott, S. Priya, and R. S. Katiyar, Appl. Phys. Lett. **97**, 252902 (2010).
[16] E. Barsoukov and J. R. Macdonald, *Impedance Spectroscopy Theory, Experiment and Applications*, second ed., (Wiley, New Jersey, 2005).
[17] C. M. Kanamadi, J. S. Kim, H. K. Yang, B. K. Moon, B. C. Choi, and J. H. Jeong, J. Alloys and Compounds **481**, 781 (2009).
[18] P. Murugavel, D. Saurel, W. Prellier, Ch. Simon, and B. Raveau, Appl. Phys. Lett. **85**, 4424 (2004).
[19] J. Wua and J. Wangb, Appl. Phys. Lett. **105**, 124107 (2009).
[20] S. Maity, D. Bhattacharya, and S. K. Ray, J. Phys. D: Appl. Phys. **44**, 095403 (2011).
[21] N. J. C. Ingle, A. Yuskauskas, R. Wicks, M. Paul, and S. Leung, J. Phys. D: Appl. Phys. **43** 133001 (2010).
[22] P. Murugavel, M. P. Singh, W. Prellier, B. Mercey, Ch. Simon, and B. Raveau, J. Appl. Phys. **97** 103914 (2005).
[23] D. C. Sinclair and A. R. West, J. Appl. Phys. **66**, 3850 (1989).
[24] N. Ortega, A. Kumar, P. Bhattacharya, S. B. Majumder, and R. S. Katiyar, Phys. Rev. B **77**, 014111 (2008).
[25] R. Schmidt, W. Eerenstein, T. Winiecki, F. D Morrison, and P. A Midgley, Phys. Rev. B **75**, 245111 (2007).
[26] J. C. C Abrantes, J. A. Labrincha, and J. R. Frade, Mate. Res. Bull. **35**, 727 (2000).
[27] Y. Tokura, A. Urushibara, Y. Moritomo, T. Arima, A. Asamitsu, G. Kido, and N. Furukawa, J. Phys. Soc. Jpn. **63**, 3931 (1994).
[28] A. K. Jonscher, J. Phys. D: Appl. Phys. **32**, R57 (1999).
[29] A. K. Jonscher, Nature (London) **264**, 673 (1977).
[30] K. Funke, Prog. Solid State Chem. **22**, 111 (1993).
[31] A. Pelaiz-Barramco, M. P. Gutierrez-Amador, A. Huanosta, and R. Valenzuela, Appl. Phys. Lett. **73**, 2039 (1998).
[32] S. R. Elliott, Adv. Phys. **36**, 135 (1987).